

Efficient geometric integrators for nonadiabatic quantum dynamics. II. The diabatic representation

Cite as: J. Chem. Phys. **150**, 204113 (2019); <https://doi.org/10.1063/1.5094046>

Submitted: 26 February 2019 . Accepted: 08 May 2019 . Published Online: 28 May 2019

Julien Roulet , Seonghoon Choi , and Jiří Vaníček 



View Online



Export Citation



CrossMark

ARTICLES YOU MAY BE INTERESTED IN

[Efficient geometric integrators for nonadiabatic quantum dynamics. I. The adiabatic representation](#)

The Journal of Chemical Physics **150**, 204112 (2019); <https://doi.org/10.1063/1.5092611>

[Quantum thermodynamics and open-systems modeling](#)

The Journal of Chemical Physics **150**, 204105 (2019); <https://doi.org/10.1063/1.5096173>

[Principal component analysis of nonequilibrium molecular dynamics simulations](#)

The Journal of Chemical Physics **150**, 204110 (2019); <https://doi.org/10.1063/1.5089636>

Lock-in Amplifiers up to 600 MHz

starting at

\$6,210



Zurich
Instruments

Watch the Video



Efficient geometric integrators for nonadiabatic quantum dynamics. II. The diabatic representation

Cite as: J. Chem. Phys. 150, 204113 (2019); doi: 10.1063/1.5094046

Submitted: 26 February 2019 • Accepted: 8 May 2019 •

Published Online: 28 May 2019



View Online



Export Citation



CrossMark

Julien Roulet,  Seonghoon Choi,  and Jiří Vaníček^{a)} 

AFFILIATIONS

Laboratory of Theoretical Physical Chemistry, Institut des Sciences et Ingénierie Chimiques, Ecole Polytechnique Fédérale de Lausanne (EPFL), CH-1015, Lausanne, Switzerland

^{a)}Electronic mail: jiri.vanicek@epfl.ch

ABSTRACT

Exact nonadiabatic quantum evolution preserves many geometric properties of the molecular Hilbert space. In the first paper of this series [“Paper I,” S. Choi and J. Vaníček, J. Chem. Phys. 150, 204112 (2019)], we presented numerical integrators of arbitrary-order of accuracy that preserve these geometric properties exactly even in the adiabatic representation, in which the molecular Hamiltonian is not separable into kinetic and potential terms. Here, we focus on the separable Hamiltonian in diabatic representation, where the split-operator algorithm provides a popular alternative because it is explicit and easy to implement, while preserving most geometric invariants. Whereas the standard version has only second-order accuracy, we implemented, in an automated fashion, its recursive symmetric compositions, using the same schemes as in Paper I, and obtained integrators of arbitrary even order that still preserve the geometric properties exactly. Because the automatically generated splitting coefficients are redundant, we reduce the computational cost by pruning these coefficients and lower memory requirements by identifying unique coefficients. The order of convergence and preservation of geometric properties are justified analytically and confirmed numerically on a one-dimensional two-surface model of NaI and a three-dimensional three-surface model of pyrazine. As for efficiency, we find that to reach a convergence error of 10^{-10} , a 600-fold speedup in the case of NaI and a 900-fold speedup in the case of pyrazine are obtained with the higher-order compositions instead of the second-order split-operator algorithm. The pyrazine results suggest that the efficiency gain survives in higher dimensions.

© 2019 Author(s). All article content, except where otherwise noted, is licensed under a Creative Commons Attribution (CC BY) license (<http://creativecommons.org/licenses/by/4.0/>). <https://doi.org/10.1063/1.5094046>

I. INTRODUCTION

The celebrated Born–Oppenheimer approximation^{1,2} assumes the separability of the nuclear and electronic motions in a molecule and provides an appealing picture of independent electronic potential energy surfaces. However, many important processes in nature³ can only be described by considering nonadiabatic couplings between these Born–Oppenheimer surfaces.^{4–7} To investigate such processes, one can abandon the Born–Oppenheimer representation and treat electrons and nuclei explicitly,^{8–10} use an exact factorization^{11,12} of the molecular wavefunction, or determine which Born–Oppenheimer states are coupled strongly^{13,14} and then solve the time-dependent Schrödinger equation with a nonadiabatically

coupled molecular Hamiltonian; below, we will only consider the third and most common strategy.

In Paper I,¹⁵ we surveyed several algorithms for the nonadiabatic quantum dynamics, applicable to higher dimensions, including Gaussian basis methods,^{16–21} variations of the multiconfigurational time-dependent Hartree (MCTDH) method,^{22–24} and sparse-grid methods.^{25,26} There are situations, however, in which the wavepacket spreads over large parts of the available Hilbert space, and then time-independent basis sets or full-grid methods can become more efficient.

As for the molecular Hamiltonian used in nonadiabatic simulations, the *ab initio* electronic structure methods typically yield the *adiabatic* potential energy surfaces, which are nonadiabatically

coupled via momentum couplings. However, in the regions of conical intersections,^{27,28} the Born-Oppenheimer surfaces become degenerate, and the nonadiabatic couplings diverge. To avoid associated problems, it is convenient to use the diabatic representation, in which the divergent momentum couplings are replaced with well-behaved coordinate couplings. Although exact diabatization is only possible in systems with two electronic states and one nuclear degree of freedom,²⁹ there exist more general, approximate diabatization procedures,^{30–32} starting with the vibronic coupling Hamiltonian model.³³ Another benefit of the diabatic representation is that it separates the Hamiltonian into a sum of kinetic energy, depending only on nuclear momenta, and potential energy, depending only on nuclear coordinates, which makes it possible to propagate the molecular wavefunction with the split-operator (SO) algorithm.^{26,34,35} The split-operator algorithm is explicit, easy to implement, and, in addition, it is an example of a geometric integrator^{36,37} because, similarly to the integrators discussed in Paper I,¹⁵ it conserves exactly many invariants of the exact solution, regardless of the convergence error of the wavefunction itself. Geometric integrators, in general, acknowledge special properties of the Schrödinger equation which differentiate it from other differential equations. Using these integrators can be likened to using a well-fitting screw-driver instead of a hammer to attach a screw. Note that the integrators for nonseparable Hamiltonians, presented in Paper I,¹⁵ are also geometric and, clearly, still applicable to the separable Hamiltonian in the diabatic representation, but the split-operator algorithm is expected to be more efficient because it is explicit.

The standard, second-order split-operator algorithm³⁴ is unitary, symplectic, stable, symmetric, and time-reversible, regardless of the size of the time step. However, to obtain highly accurate results, the standard algorithm requires using a small time step because it has only second-order accuracy. There exist much more efficient algorithms, such as the short-iterative Lanczos algorithm,^{38–40} which has an exponential convergence with respect to the time step and also conserves the norm and energy, but not the inner product (because it is nonlinear) and other geometric properties.

To address the low accuracy of the second-order split-operator algorithm and the nonconservation of geometric properties by other more accurate methods, various higher-order split-operator integrators have been introduced,^{41–44} some of which allow complex time steps^{44–46} or commutators of the kinetic and potential energies in the exponent,^{47–49} thus reducing the number of splitting steps. Here, we explore one type of higher-order integrators, designed for nonadiabatic dynamics in the diabatic basis, which we have implemented using the recursive triple-jump^{42,43} and Suzuki-fractal,⁴² as well as several nonrecursive, “optimal” compositions of the second-order split-operator algorithm. While the recursive compositions permit an automated generation of integrators of arbitrary even order in the time step,^{36,37,42,43,50,51} the efficiency of higher-order algorithms is sometimes questioned because the number of splitting steps grows exponentially with the order of accuracy, and consequently, so does the computational cost of a single time step. Motivated by this dilemma, we have explored the convergence and efficiency of the higher-order compositions using a one- and three-dimensional systems, concluding that, despite the increasing number of splittings, the higher-order methods become the most efficient if higher accuracy of the solution is required and that this gain in efficiency survives in higher dimensions. We have also confirmed

that all composed methods are unitary, symplectic, stable, symmetric, and time-reversible. A final benefit of the higher-order methods is the simple, abstract, and general implementation of the compositions of the second-order split-operator algorithm; indeed, even this “elementary” method is a composition of simpler, first-order algorithms.^{26,35}

One of the only challenges of implementing the split-operator algorithm for nonadiabatic dynamics in the diabatic representation is the exponentiation of the potential energy operator, which is nondiagonal in the electronic degrees of freedom (in contrast to the diagonal kinetic energy operator). We, therefore, explored several methods for the exponentiation of nondiagonal matrices.

The main disadvantage of the split-operator algorithm and its compositions is that their use is restricted to separable Hamiltonians. To compare them with the integrators from Paper I,¹⁵ we cannot use the adiabatic representation but instead must perform the comparison in the diabatic representation, where the compositions of the explicit split-operator algorithm are, as expected, much more efficient than the more generally applicable compositions¹⁵ of the implicit trapezoidal rule (the Crank-Nicolson method^{52,53}) from Paper I.¹⁵ Nevertheless, the comparison serves as a higher-dimensional test of integrators from Paper I¹⁵ and confirms that, in contrast to the split-operator compositions, the integrators from Paper I¹⁵ conserve also the energy exactly.

The remainder of this paper is organized as follows: In Sec. II, after reviewing the geometric properties of the exact evolution operator, we discuss the lack of symmetry and time-reversibility in the first-order split-operator algorithms and the recovery of these properties in the symmetric compositions. Next, we describe several strategies for reducing the computational cost and memory requirements by pruning redundant splitting coefficients generated automatically by the symmetric compositions. After presenting the dynamic Fourier method for its ease of implementation and the exponential convergence with the grid density, we briefly discuss the molecular Hamiltonian in the diabatic representation. In Sec. III, the convergence properties and conservation of geometric invariants by various methods are analyzed numerically on a one-dimensional two-surface model⁵⁴ of NaI and a three-dimensional three-surface model of pyrazine,⁵⁵ both in the diabatic representation. Section IV concludes the paper.

II. THEORY

A. Geometric properties of the exact evolution operator

The time-dependent Schrödinger equation

$$i\hbar \frac{d\psi(t)}{dt} = \hat{H}\psi(t) \quad (1)$$

with a time-independent Hamiltonian \hat{H} and initial condition $\psi(0)$ has the formal solution $\psi(t) = \hat{U}(t)\psi(0)$, where $\hat{U}(t)$ is the evolution operator. While in Paper I,¹⁵ we considered general Hamiltonian operators $\hat{H} \equiv H(\hat{q}, \hat{p})$, here we require that the Hamiltonian be separable as

$$\hat{H} \equiv \hat{T} + \hat{V} \equiv T(\hat{p}) + V(\hat{q}) \quad (2)$$

into a sum of kinetic and potential energies, which depend, respectively, only on the momentum \hat{p} and position \hat{q} operators.

The exact evolution operator

$$\hat{U}(t) = e^{-i\hat{H}t/\hbar} = e^{-i[T(\hat{p})+V(\hat{q})]t/\hbar} \quad (3)$$

is linear, unitary, symplectic, symmetric, time-reversible, stable, and conserves the norm, inner product, and energy. Because these properties are desirable also in approximate numerical evolution operator $\hat{U}_{\text{appr}}(t)$, let us define them briefly.

An operator \hat{U} is said to *preserve the norm* if $\|\hat{U}\psi\| = \|\psi\|$ for all ψ and to *preserve the inner product* if $\langle \hat{U}\psi | \hat{U}\phi \rangle = \langle \psi | \phi \rangle$ for all ψ and ϕ . For linear operators \hat{U} , these two properties are equivalent, whereas for general, possibly nonlinear operators, conservation of the inner product implies linearity³⁶ and hence the conservation of norm, but norm conservation implies neither linearity nor conservation of the inner product. An operator \hat{U} is said to be *unitary* if $\hat{U}^\dagger = \hat{U}^{-1}$, where \hat{U}^\dagger is the Hermitian adjoint. An operator \hat{U} is called *symplectic* if $\omega(\hat{U}\psi, \hat{U}\phi) = \omega(\psi, \phi)$, where $\omega(\psi, \phi)$ is a *symplectic two-form*, i.e., a nondegenerate skew-symmetric bilinear form. We will only consider the symplectic two-form defined as²⁶ $\omega(\psi, \phi) := -2\hbar \text{Im}\langle \psi | \phi \rangle$, which is conserved if the inner product is conserved. \hat{U} is said to *conserve energy* if $\langle \hat{H} |_{\hat{U}\psi} = \langle \hat{H} |_\psi$, where $\langle \hat{A} |_\psi := \langle \psi | \hat{A} | \psi \rangle$ denotes the expectation value of operator \hat{A} in the state ψ . Finally, an *adjoint* $\hat{U}(t)^*$ of an evolution operator $\hat{U}(t)$ is defined as $\hat{U}(t)^* := \hat{U}(-t)^{-1}$. An evolution operator is said to be *symmetric* if^{36,37} $\hat{U}(t)^* = \hat{U}(t)$ and *time-reversible* if^{36,37} $\hat{U}(-t)\hat{U}(t)\psi = \psi$. For the definition of stability and a more detailed presentation and discussion of other properties, see Sec. II A of Paper I.¹⁵

B. First-order split-operator methods

In approximate propagation methods, the state at time $t + \Delta t$ is obtained from the state at time t using the relation

$$\psi(t + \Delta t) = \hat{U}_{\text{appr}}(\Delta t)\psi(t),$$

where $\hat{U}_{\text{appr}}(\Delta t)$ is an approximate time evolution operator and Δt is the numerical time step. Depending on the order of kinetic and potential propagations, the approximate evolution operator is

$$\hat{U}_{\text{VT}}(\Delta t) := e^{-\frac{i}{\hbar}\Delta t\hat{V}} e^{-\frac{i}{\hbar}\Delta t\hat{T}} \quad (4)$$

in the *VT split-operator algorithm* and

$$\hat{U}_{\text{TV}}(\Delta t) := e^{-\frac{i}{\hbar}\Delta t\hat{T}} e^{-\frac{i}{\hbar}\Delta t\hat{V}} \quad (5)$$

in the *TV split-operator algorithm*. Both \hat{U}_{VT} and \hat{U}_{TV} are unitary, symplectic, stable, but only first-order in the time step Δt .

Neither method conserves energy because neither evolution operator commutes with the Hamiltonian. Neither method is symmetric; in fact, they are adjoints of each other. Hence, neither method is time-reversible. These properties are justified in Appendix A and summarized in Table I.

Although the first-order split-operator algorithms are not time-reversible, composing them in a specific way leads to time-reversible integrators of arbitrary order of accuracy in the time step.

C. Recovery of geometric properties by composed methods

Composing the two first-order split-operator algorithms, each for a time step $\Delta t/2$, yields a symmetric second-order method.³⁴ Depending on the order of composition, one obtains either

$$\hat{U}_{\text{VTV}}(\Delta t) := \hat{U}_{\text{VT}}(\Delta t/2)\hat{U}_{\text{TV}}(\Delta t/2) \quad (6)$$

in the *VTV algorithm* or

$$\hat{U}_{\text{TVT}}(\Delta t) := \hat{U}_{\text{TV}}(\Delta t/2)\hat{U}_{\text{VT}}(\Delta t/2) \quad (7)$$

in the *TVT algorithm*. Both are explicit, unitary, symplectic, stable, symmetric, and time-reversible, regardless of the size of the time step. Neither evolution operator commutes with the Hamiltonian, and therefore, neither method conserves energy exactly. These properties are again justified in Appendix A and summarized in Table I.

D. Symmetric composition schemes for symmetric methods

As discussed in Paper I,¹⁵ composing any symmetric second-order method (such as one of those of Sec. II C) with appropriately chosen time steps leads to symmetric integrators of arbitrary order of accuracy.^{36,37,42,43} More precisely, there are a natural number M and real numbers γ_n , $n = 1, \dots, M$, called *composition coefficients*, such that $\gamma_1 + \dots + \gamma_M = 1$ and such that for any symmetric evolution operator $\hat{U}_p(\Delta t)$ of an even order p , composing this symmetric evolution operator with coefficients γ_n yields a symmetric integrator of order $p + 2$,

$$\hat{U}_{p+2}(\Delta t) := \hat{U}_p(\gamma_M\Delta t)\dots\hat{U}_p(\gamma_1\Delta t).$$

The simplest composition schemes (see Fig. 2 of Ref. 15) are the triple jump^{41–43,57} with $M = 3$ and Suzuki's fractal⁴² with $M = 5$. Both are *symmetric compositions*, meaning that $\gamma_{M+1-n} = \gamma_n$. Because larger time steps can be used for calculations using Suzuki's fractal, this composition is sometimes more efficient than the triple-jump composition, despite requiring more composition steps (see

TABLE I. Geometric properties and computational cost of the first-order and recursively composed second-order split-operator (SO) algorithms. Cost (here before speedup by pruning splitting coefficients) is measured by the number of fast Fourier transforms required per time step (see Sec. II C). n is the number of recursive compositions and C is the total number of composition steps per time step ($C = 3^n$ for the triple jump,^{42,43} $C = 5^n$ for Suzuki's fractal⁴²). + or – denotes that the geometric property of the exact evolution operator is or is not preserved.

Method	Order	Unitary	Symplectic	Commutates with \hat{H}	Energy cons.	Symmetric	Time-reversible	Stable	Cost
1st order SO	1	+	+	–	–	–	–	+	2
2nd order SO	$2(n + 1)$	+	+	–	–	+	+	+	$2C$

Ref. 15 for a numerical example). For specific orders of convergence, more efficient nonrecursive composition schemes exist and will be referred to as “optimal.” These were implemented according to Kahan and Li⁵⁸ for the 6th and 8th orders and according to Sofroniou and Spaletta⁵⁹ for the 10th order (see Sec. II D of Paper I¹⁵ for more details about composition methods).

E. Compositions of split-operator algorithms

The split-operator algorithm is applicable if the Hamiltonian \hat{H} can be written as a sum

$$\hat{H} = \hat{A} + \hat{B} \quad (8)$$

of operators \hat{A} and \hat{B} with evolution operators, $\hat{U}_{\hat{A}}(t) = \exp(-it\hat{A}/\hbar)$ and $\hat{U}_{\hat{B}}(t) = \exp(-it\hat{B}/\hbar)$, whose actions on ψ can be evaluated exactly. A general split-operator evolution operator can be expressed as

$$\hat{U}_{\hat{A}+\hat{B}}^{\text{SO}}(\Delta t) = \hat{U}_{\hat{B}}(b_N \Delta t) \hat{U}_{\hat{A}}(a_N \Delta t) \cdots \hat{U}_{\hat{B}}(b_1 \Delta t) \hat{U}_{\hat{A}}(a_1 \Delta t),$$

where N is the number of splitting steps and a_j and b_j are the splitting coefficients associated with the operators \hat{A} and \hat{B} . These coefficients, in general, satisfy the identity $\sum_{j=1}^N a_j = \sum_{j=1}^N b_j = 1$ and are $a_1 = b_1 = 1$ for the first-order VT and TV algorithms⁶⁰ and

$$a_1 = a_2 = \frac{1}{2}, \quad b_1 = 1, \quad b_2 = 0 \quad (9)$$

for the second-order VTV or TVT algorithms.⁶¹

Because the second-order split-operator algorithm⁶¹ is symmetric, it can be composed by any of the composition schemes discussed in Sec. II D. For example, the splitting coefficients of a fourth-order method are

$$\begin{aligned} a_1 = a_2 = \frac{1}{2(2-2^{1/3})}, \quad a_3 = -\frac{2^{1/3}}{2(2-2^{1/3})}, \\ b_1 = \frac{1}{2-2^{1/3}}, \quad b_3 = -\frac{2^{1/3}}{2-2^{1/3}}, \quad b_2 = b_6 = 0 \end{aligned} \quad (10)$$

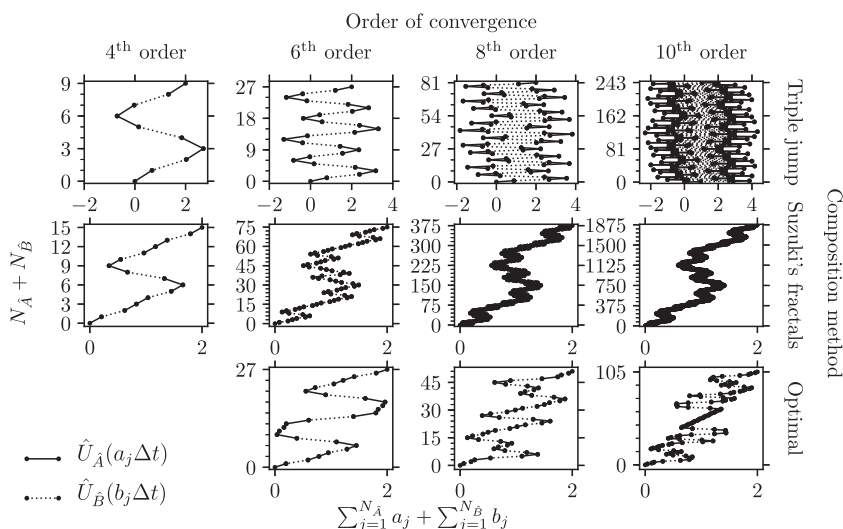


FIG. 1. Split-operator algorithms composed by the recursive (triple jump and Suzuki’s fractal) and nonrecursive “optimal” composition schemes shown in Fig. 2 of Paper I.¹⁵ In other words, each elementary method $\hat{U}(\gamma_n \Delta t)$ (solid line segment in Fig. 2 of Paper I¹⁵) is replaced by a second-order split-operator algorithm $\hat{U}_{\hat{A}}(\gamma_n \Delta t/2) \hat{U}_{\hat{B}}(\gamma_n \Delta t) \hat{U}_{\hat{A}}(\gamma_n \Delta t/2)$, represented here by a triple of consecutive solid, dotted, and solid line segments. Solid line segments represent $\hat{U}_{\hat{A}}(\gamma_n \Delta t/2)$, whereas the dotted line segments represent $\hat{U}_{\hat{B}}(\gamma_n \Delta t)$. $N_{\hat{O}}$ is the number of actions of $\hat{U}_{\hat{O}}$ on ψ .

with $N = 6$ if the triple-jump composition scheme is used, and

$$\begin{aligned} a_1 = a_2 = a_3 = a_4 = \frac{1}{2(4-4^{1/3})}, \quad a_5 = -\frac{4^{1/3}}{2(4-4^{1/3})}, \\ b_1 = b_3 = \frac{1}{4-4^{1/3}}, \quad b_2 = b_4 = b_{10} = 0, \quad b_5 = -\frac{4^{1/3}}{4-4^{1/3}}, \end{aligned} \quad (11)$$

with $N = 10$ if Suzuki’s fractal is used instead. The remaining coefficients are obtained from symmetry as

$$a_{N-j+1} = a_j, \quad b_{N-j} = b_j. \quad (12)$$

Both composition procedures can be applied recursively to obtain higher-order split-operator algorithms. These as well as the optimally composed algorithms of up to the tenth order are represented pictorially in Fig. 1.

All compositions of the second-order VTV or TVT split-operator algorithms are unitary, symplectic, and stable; all symmetric compositions are symmetric and, therefore, time-reversible. The proof of this statement is a special case of the general proof of a corresponding theorem for the composition of geometric integrators in Paper I.¹⁵

F. Pruning splitting coefficients

Many b_j coefficients of the higher-order integrators obtained by recursive composition of the second-order split-operator algorithm are zero [for example, see Eqs. (10) and (11)]. The computational cost can be reduced by “pruning,” i.e., removing the splitting steps corresponding to $b_j = 0$ and merging the consecutive actions of $\hat{U}_{\hat{A}}(a_j \Delta t)$ and $\hat{U}_{\hat{A}}(a_{j+1} \Delta t)$. If $b_j = 0$ and $j \neq N$, the splitting coefficients are modified as

$$\begin{aligned} \tilde{b}_k &= b_{k+1}, \quad \text{for } j \leq k \leq N-1, \\ \tilde{a}_j &= a_j + a_{j+1}, \\ \tilde{a}_k &= a_{k+1}, \quad \text{for } j+1 \leq k \leq N-1, \\ \tilde{N} &= N-1, \end{aligned} \quad (13)$$

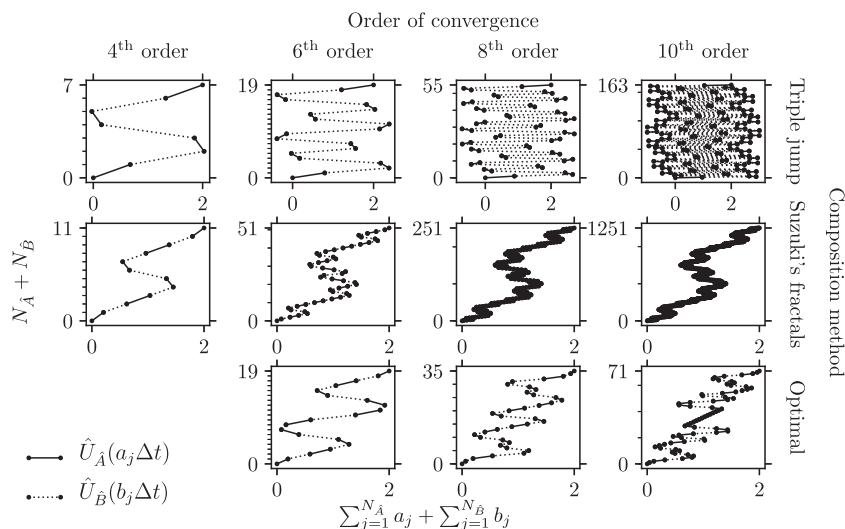


FIG. 2. Composed split-operator algorithms from Fig. 1 after removing zero splitting coefficients and merging adjacent coefficients, i.e., after each two adjacent solid line segments representing $\hat{U}_A(\gamma_{n+1}\Delta t/2)\hat{U}_A(\gamma_n\Delta t/2)$ in Fig. 1 are merged into a single solid line segment representing $\hat{U}_A((\gamma_n + \gamma_{n+1})\Delta t/2)$.

in order to merge the j th and $(j + 1)$ th steps. The composed methods after the merge are exhibited in Fig. 2, and the reduction in the number N of splitting steps, which measures the computational cost, is summarized in Table II.

For a time-independent separable Hamiltonian, one can either precompute and store the evolution operators, $\hat{U}_A(a_j\Delta t)$ and $\hat{U}_B(b_j\Delta t)$ or compute them on the fly. The former approach is more memory intensive than the latter, which does not store any evolution

operators, but the computational cost is reduced since the evolution operators are only computed once at initialization. To alleviate the memory requirement of the former approach, one can exploit the repetition of certain splitting coefficients, which is obvious from Eqs. (10) and (11) and Fig. 2. If either \hat{A} or \hat{B} is time-dependent, it is always beneficial to compute the corresponding evolution operator pertaining to the time-dependent operator on the fly because no reduction in computational cost is possible by precomputing the evolution operators.

The effort spent in searching for repeated coefficients is reduced if the symmetries of the composition scheme and of the elementary method are exploited [see Eq. (12)]. The repeated coefficients are then identified from only half of the original coefficients a_j and b_j .

Once identified, only the unique evolution operators $\hat{U}_A(a_j^{\text{uniq}}\Delta t)$ and $\hat{U}_B(b_j^{\text{uniq}}\Delta t)$ are stored in arrays of lengths N_a^{uniq} and N_b^{uniq} , together with the information when to apply them, stored in integer arrays I^a and I^b of length N , containing the indices in unique coefficient arrays, i.e.,

$$1 \leq I_j^a \leq N_a^{\text{uniq}}, \quad 1 \leq I_j^b \leq N_b^{\text{uniq}}. \quad (14)$$

Exploiting the repeated coefficients, the number of stored evolution operators reduces from $2N$ to $N_a^{\text{uniq}} + N_b^{\text{uniq}}$ (see Table II).

G. Dynamic Fourier method

To propagate a wavepacket $\psi(t)$ with any split-operator algorithm (see Secs. II B–II D), only the actions of the kinetic (\hat{U}_T) and potential (\hat{U}_V) evolution operators on $\psi(t)$ are required, where

$$\hat{U}_T(\Delta t) := e^{-i\Delta t T(\hat{p})/\hbar} \quad \text{and} \quad \hat{U}_V(\Delta t) := e^{-i\Delta t V(\hat{q})/\hbar}.$$

Since \hat{U}_T and \hat{U}_V are diagonal in the momentum and position representations, respectively, their action on $\psi(t)$ is easy to evaluate in the appropriate representation. This is the main idea of the dynamic Fourier method,^{34,35,62,63} in which the representation of $\psi(t)$ is repeatedly changed, as needed, via the fast Fourier transform (for more details, see Sec. II E of Paper I¹⁵).

TABLE II. Computational cost and memory requirement of the composed split-operator algorithms before and after pruning (i.e., removing zero coefficients and merging adjacent coefficients) and identifying repeated coefficients. The computational cost is measured by $N_A + N_B$, where N_O is the number of actions of \hat{U}_O on the wavepacket. The memory requirement before and after pruning is $N_A + N_B$ and after identifying repeated coefficients decreases to $N_a^{\text{uniq}} + N_b^{\text{uniq}}$.

Composition method	Order	$N_A + N_B$		N_a^{uniq}	N_b^{uniq}
		before merge ^a	after merge ^b		
Elementary methods	1	2	2	1	1
	2	3	3	1	1
Triple jump	4	9	7	2	2
	6	27	19	4	4
	8	81	55	8	8
	10	243	163	16	16
Suzuki's fractal	4	15	11	3	2
	6	75	51	6	4
	8	375	251	12	8
	10	1875	1251	24	16
Optimal	6	27	19	5	5
	8	51	35	9	9
	10	105	71	18	18

^a $N_A = 2N_B$ for order ≥ 2 .

^b $N_A = N_B + 1$ for order ≥ 2 .

In the numerical examples below, the Fourier transform was performed using the Fastest Fourier Transform in the West 3 (FFTW3) library.⁶⁴ Although its accuracy is sufficient for most applications, small deviations from unitarity, which were due to the high number of repeated application of the forward and backward Fourier transforms, affected the most converged calculations. To reduce the nonunitarity, we used the long-double instead of the default double precision version of FFTW3.

H. Molecular Hamiltonian in the diabatic basis

The molecular Hamiltonian in the diabatic basis can be expressed as

$$\hat{H} = \frac{1}{2} \hat{p}^T \cdot m^{-1} \cdot \hat{p} \mathbf{1} + \mathbf{V}(\hat{q}), \quad (15)$$

where m is the diagonal $D \times D$ nuclear mass matrix, D is the number of nuclear degrees of freedom, and \mathbf{V} is the potential energy. In Eq. (15), the dot \cdot denotes the matrix product in nuclear D -dimensional vector space, the hat $\hat{\cdot}$ represents a nuclear operator, and the **bold** font indicates an electronic operator, i.e., an $S \times S$ matrix, where S is the number of included electronic states. Using the dynamic Fourier method, each evaluation of the action of the pair $\hat{U}_{\hat{V}}(t_V)$ and $\hat{U}_{\hat{T}}(t_T)$ on a molecular wavepacket $\psi(t)$, which now becomes an S -component vector of nuclear wavepackets (one on each surface), involves two changes of the wavepacket's representation. The above-mentioned nonunitarity of the solution, partially due to the numerical implementation of the FFT algorithm, was made worse by the matrix exponential required for evaluating the potential evolution operator $\hat{U}_{\hat{V}}(t_V)$, which contains offdiagonal couplings between the electronic states. Although we tried different approaches for matrix exponentiation, including Padé approximants^{65,66} and exponentiating a diagonal matrix obtained with the QR decomposition^{65,67} or with the Jacobi method,⁶⁵ none of the three methods was better than the others in reducing the nonunitarity. Since both in the NaI and pyrazine models, only 2×2 matrices are relevant, and since for such matrices, the Jacobi method yields already after one iteration the analytically exact result for the exponential, we used the Jacobi method for all results in Sec. III. Note, however, that the other two methods (based on Padé approximants or QR decomposition), while not exact in the two models used in this paper, converge, in general, faster than the Jacobi method and are, therefore, preferred in systems with more than two coupled electronic states.

I. Trapezoidal rule and implicit midpoint method

In addition to nonconservation of energy, the main disadvantage of the split-operator algorithms is that they can be applied to nonadiabatic dynamics only in the diabatic representation. Yet, there exist closely related, arbitrary-order geometric integrators, discussed in Paper I,¹⁵ which, in addition, conserve energy and are applicable both in the diabatic and adiabatic representations. These integrators are, like the higher-order split-operator algorithms, based on recursive symmetric composition (see Sec. II D) of the second-order trapezoidal rule (Crank-Nicolson method^{52,53}) or the implicit midpoint method, both of which are, themselves, compositions of the explicit and implicit Euler methods [see Eqs. (13), (14), (18), and (19) of Paper I¹⁵]. Due to the presence of

implicit steps, the trapezoidal rule, implicit midpoint method, as well as their compositions require solving large, although sparse, linear systems iteratively,¹⁵ and, as a result, in the diabatic representation are expected to be significantly less efficient than the explicit split-operator algorithms of the same order of accuracy. These integrators are, again, most naturally implemented in conjunction with the dynamic Fourier method described in Sec. II G; the only difference being that one must evaluate the operation $(\hat{T} + \hat{V})\psi$ instead of $\hat{U}_{\hat{T}}\psi$ and $\hat{U}_{\hat{V}}\psi$. More details about these higher-order integrators can be found in Paper I,¹⁵ which discusses their geometric properties and studies their efficiency in applications to nonadiabatic quantum dynamics in the adiabatic representation, in which the molecular Hamiltonian is nonseparable.

III. NUMERICAL EXAMPLES

To test the geometric and convergence properties of the split-operator algorithms presented in Secs. II B–II D, we used these integrators to simulate the nonadiabatic quantum dynamics in a one- and three-dimensional systems.

A. One-dimensional model of NaI

This model is a diabaticized version of the one presented in Paper I,¹⁵ i.e., a one-dimensional two-surface model⁵⁴ of the NaI molecule. We used the same initial and final times, and the same approximations for the initial state and for the molecule-field interactions as in Paper I.¹⁵ For detailed calculation parameters, see Sec. III of Ref. 15.

The top panel of Fig. 3 shows the two diabatic potential energy surfaces as well as the initial wavepacket at $t = 0$ and the ground- and excited-state components of the final wavepacket at the final time $t_f = 10\,500$ a.u. The population dynamics of NaI, displayed in the middle and bottom panels of Fig. 3, shows that after passing this crossing, most of the population jumps to the other diabatic state, while a small fraction remains in the original, dissociative diabatic state. On the scale visible in the figure, the converged populations obtained with the VTV and TVT split-operator algorithms agree with each other and also with the results of the trapezoidal rule and implicit midpoint method (middle panel). Moreover, the results of the triple-jump, Suzuki-fractal, and optimal compositions of the second-order VTV algorithm agree with each other (bottom panel).

For a quantitative comparison of various algorithms, it is necessary to compare their convergence errors at the final time t_f . As in Paper I,¹⁵ the convergence error at time t_f as a function of the time step Δt is measured by the L_2 -norm error $\|\psi_{\Delta t}(t_f) - \psi_{\Delta t/2}(t_f)\|$, where $\psi_{\tau}(t_f)$ represents the wavepacket propagated with a time step τ . This error is shown in Fig. 4, which confirms, for each algorithm, the asymptotic order of convergence predicted in Secs. II B–II D. For clarity, in this and all remaining figures, only the VT algorithm and compositions of the VTV algorithm are compared because the corresponding results of the TV algorithm and compositions of the TVT algorithm behave similarly. The top panel of Fig. 4 compares all methods, whereas the bottom left-hand panel compares only the different orders of the triple-jump composition and the bottom right-hand panel compares only different composition schemes with the sixth-order convergence. Similarly to the results in the adiabatic basis,¹⁵ the prefactor of the error is the largest for

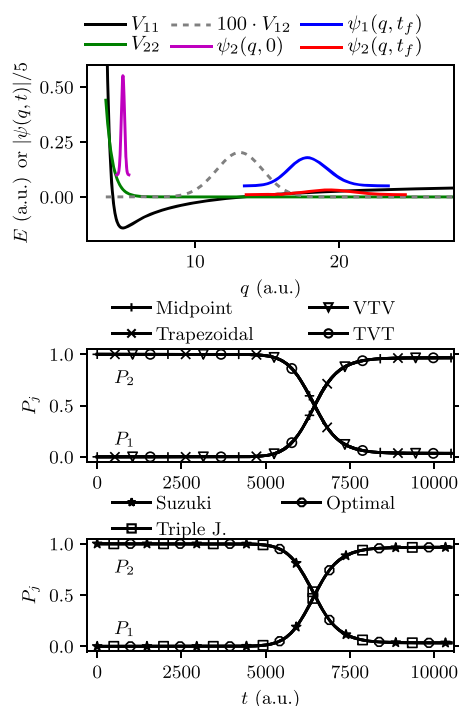


FIG. 3. Nonadiabatic dynamics of NaI. Top: Diabatic potential energy surfaces with the initial and final nuclear wavepacket components in the two diabatic electronic states (the initial ground-state component is not shown because it was zero: $\psi_1(q, 0) = 0$). Middle: Populations of NaI in the two diabatic states computed with four different second-order methods. Bottom: Populations computed with three different sixth-order compositions of the VTV algorithm. Populations were propagated with a time step $\Delta t = 0.01$ a.u. for the second-order methods and $\Delta t = 82.03125$ a.u. for the sixth-order methods, i.e., much more frequently than the markers suggest. The time step guaranteed wavepacket convergence errors below $\approx 10^{-5}$ in all methods.

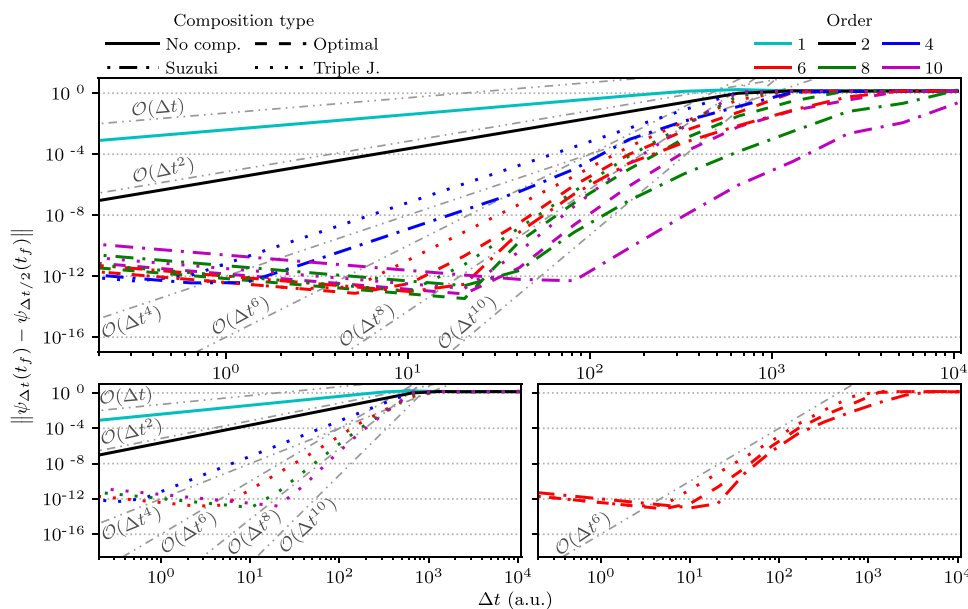


FIG. 4. Convergence of the molecular wavefunction as a function of the time step. The wavefunction was propagated with the VT algorithm or with the compositions of the VTV algorithm. Gray straight lines indicate various predicted orders of convergence $\mathcal{O}(\Delta t^m)$. Top: all discussed methods, bottom left: methods composed with the triple-jump scheme, and bottom right: sixth-order methods.

the triple-jump,^{42,43} intermediate for the optimal,⁵⁸ and smallest for Suzuki-fractal composition. The figure also shows that for the smallest time steps, the error starts to increase again. This is due to the accumulating numerical error of the fast Fourier transform, which eventually outweighs the error due to time discretization. As a result, the predicted asymptotic order of convergence cannot be observed for some methods because it is only reached for very small time steps.

While the probability density has a classical analogue, the phase of the wavefunction is a purely quantum property. As a consequence, an accurate evaluation of the phase is very important in the calculation of electronic spectra and in other situations, where quantum effects play a role. To investigate the convergence of the phase as a function of the time step, we used the phase of wavefunction at the maximum of the probability density (for a precise definition, see Paper I¹⁵). Figure 5 displays the convergence of the error of the phase for the triple-jump compositions and confirms that the order of convergence is the same as for the wavefunction itself (bottom left-hand panel of Fig. 4).

Because the number of composition steps depends on the composition scheme and increases with the order, the efficiency of an algorithm is not determined solely by the convergence error for a given time step Δt . It is, therefore, essential to compare directly the efficiency of the different algorithms. Figure 6 displays the wavefunction convergence error of each algorithm as a function of the computational cost, measured with the central processing (CPU) time. A comparison of the compositions of the VTV split-operator algorithm in the top panel of Fig. 6 shows that the fourth-order Suzuki composition already takes less CPU time to achieve convergence error 10^{-2} than does the elementary VTV algorithm. To reach errors below 10^{-2} , it is more efficient to use some of the fourth or higher-order integrators. Remarkably, the CPU time required to reach an error of 10^{-10} is roughly 600 times longer for the basic VTV algorithm than for its optimal 6th-order composition. The bottom right-hand panel of Fig. 6 confirms the prediction that the optimal

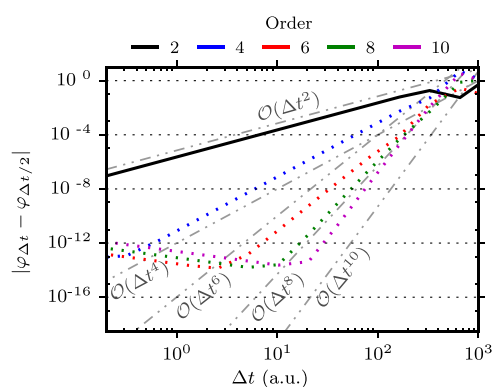


FIG. 5. Convergence error of the phase of the wavepacket as a function of the time step for the triple-jump compositions. Gray straight lines indicate various predicted orders of convergence $\mathcal{O}(\Delta t^n)$.

compositions are the most efficient among composition methods of the same order.

Convergence curves in Figs. 4–6 were obtained using the long-double precision for the FFTW3 algorithm, which lowered the error

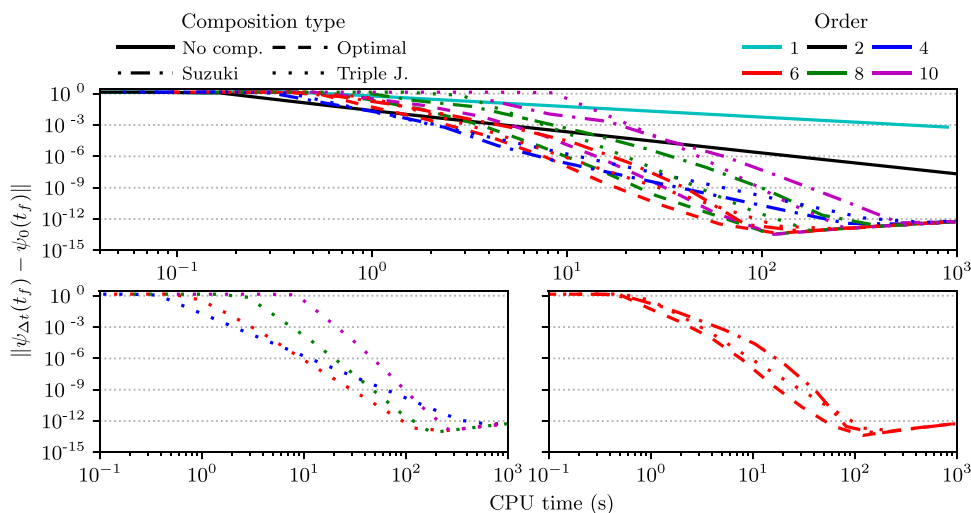


FIG. 6. Efficiency of the VT algorithm and of various compositions of the VTV algorithm shown using the dependence of the convergence error on the computational cost. Top: all methods, bottom left: triple-jump compositions, bottom right: sixth-order methods. The reference wavefunction $\psi_0(t_f)$ was chosen as the most accurate point in Fig. 4, i.e., the wavefunction obtained using the optimal eighth-order composition with a time step $\Delta t = t_f/2^9$.

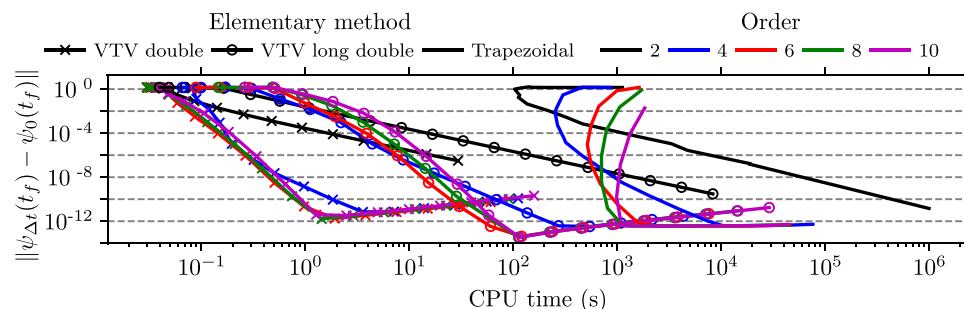


FIG. 7. Efficiency of the optimal compositions of the trapezoidal rule and of the VTV split-operator algorithm applied to the NaI model. For the trapezoidal rule, only the double precision version of the FFTW3 fast Fourier transform was used, while for the VTV split-operator algorithm, both double and long-double precision versions are compared. The “exact” reference wavefunction $\psi_0(t_f)$ is the same as in Fig. 6. The result of the elementary second-order trapezoidal rule was extrapolated below the error of $\approx 10^{-7}$ using the line of best fit. As for the fourth-order algorithms, Suzuki’s fractal is considered as the “optimal” composition scheme.

accumulation resulting from the nonunitarity of the FFTW3 Fourier transform. If high accuracy is not desired, the double precision of the FFTW3 algorithm can be used instead, resulting in much more efficient higher-order algorithms. This is shown for the NaI model in Fig. 7, which compares the efficiency of the optimal compositions of the VTV algorithm evaluated either with the double or long-double implementation of the FFTW3, and also with the corresponding compositions of the trapezoidal rule (for which the double precision of FFTW3 was sufficient). Even the more expensive, long-double precision calculation with the compositions of the VTV algorithm are faster than the corresponding double precision calculations with the trapezoidal rule, which requires an expensive iterative solution of a system of linear equations. In particular, the sixth-order optimal composition of the VTV algorithm reaches a convergence error of 10^{-10} 40 times faster than the same composition of the trapezoidal rule (see Fig. 7) and 30 000 times faster than the elementary trapezoidal rule (see Figs. 6 and 7).

Note that the dependence of CPU time on the error in Fig. 7 is not monotonous for the compositions of the trapezoidal rule because the convergence of the numerical solution to the system of linear equations required more iterations for larger time steps; as a result, both the error and CPU time increased for time steps larger than a certain critical value.

To check that the increased efficiency of higher-order compositions is not achieved by sacrificing the conservation of geometric invariants, we analyzed, using the NaI model, the conservation of norm, symplectic two-form, energy, and time reversibility. Conservation of the norm and symplectic two-form and nonconservation of energy by all split-operator algorithms are demonstrated in panels (a)–(c) of Fig. 8. The tiny residual errors ($<10^{-12}$ in all cases) result

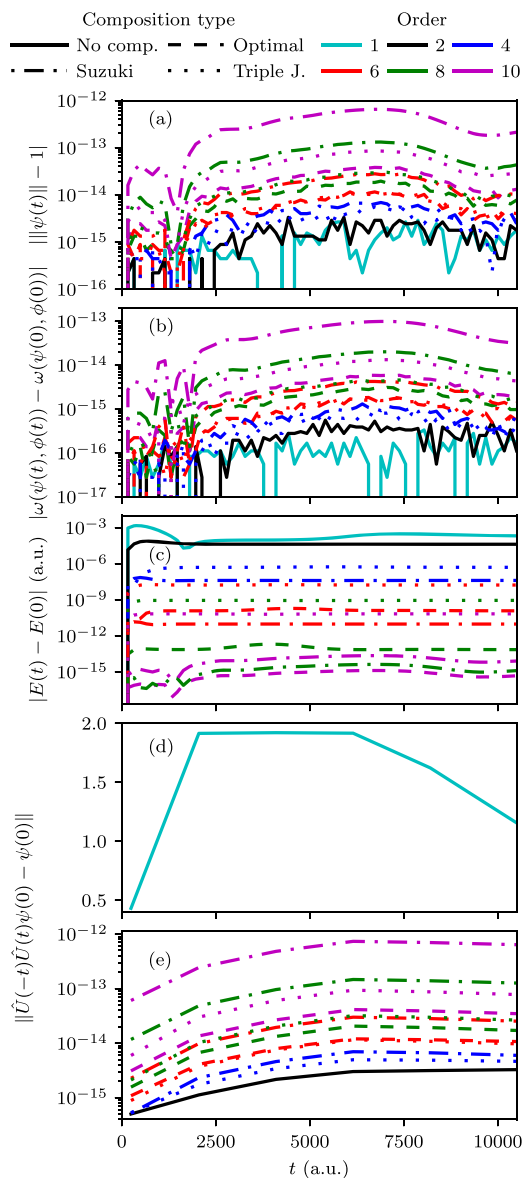


FIG. 8. Conservation of geometric properties by various algorithms: (a) norm, (b) symplectic two-form, (c) energy, and (d) and (e) time reversibility. $\phi(0)$ is a Gaussian wavepacket with $q_0 = 5.05$ a.u., $p_0 = 2.5$ a.u., and σ_0 identical to that of $\psi(0)$. Time reversibility was measured by the distance of the initial state $\psi(0)$ from a forward-backward propagated state, i.e., the state $\psi(0)$ propagated first forward in time for time t and then backward in time for time t . The NaI model and a time step $\Delta t = t_f/2^7$ a.u. were used in all calculations.

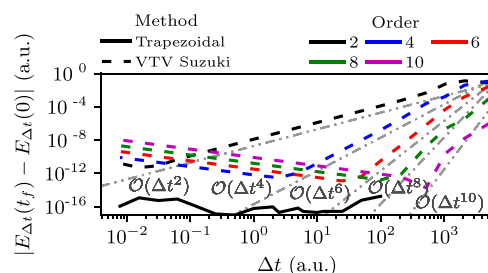


FIG. 9. Energy conservation as a function of the time step in simulations of the nonadiabatic dynamics of NaI. Gray straight lines indicate various orders of convergence $\mathcal{O}(\Delta t^n)$.

from accumulated numerical errors of the FFT and matrix exponentiation (see Sec. II G). Panels (d) and (e) confirm, on one hand, that the first-order split-operator algorithm is not time-reversible, and on the other hand, that the second-order VTV algorithm together with all its compositions are exactly time-reversible; the tiny residual errors are again due to accumulated numerical errors of the FFT and matrix exponentiation.

The nonconservation of energy by the split-operator algorithms is further inspected in Fig. 9, showing the error of energy as a function of the time step. For the Suzuki-fractal compositions of the VTV algorithm, the energy is only conserved approximately; its conservation follows the order of convergence of the integrator, as indicated by the gray lines. By contrast, the trapezoidal rule conserves the energy to machine accuracy, regardless of the size of the time step.

B. Three-dimensional model of pyrazine

To investigate how the dimensionality of the system affects the efficiency of various algorithms, we also performed analogous simulations of a three-dimensional three-surface vibronic coupling model of pyrazine. The model, which includes only the normal modes Q_1 , Q_{6a} , and Q_{10a} , was constructed by following the procedure from Ref. 55 with the experimental values from Ref. 68 for the vertical excitation energies. Thirty-two equidistant grid points between $q = -7$ a.u. and $q = 7$ a.u. were included for each vibrational

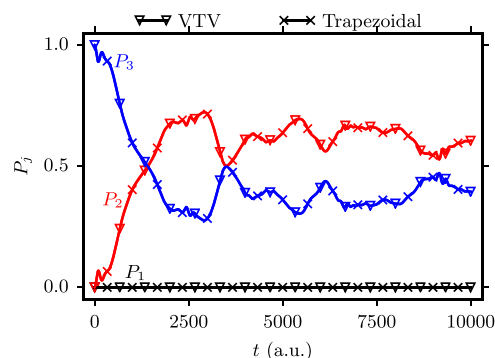


FIG. 10. Population dynamics of pyrazine obtained using the sixth-order optimal compositions of the trapezoidal rule and VTV algorithm. The same time step $\Delta t = t_f/2^5 600$ was used for both calculations.

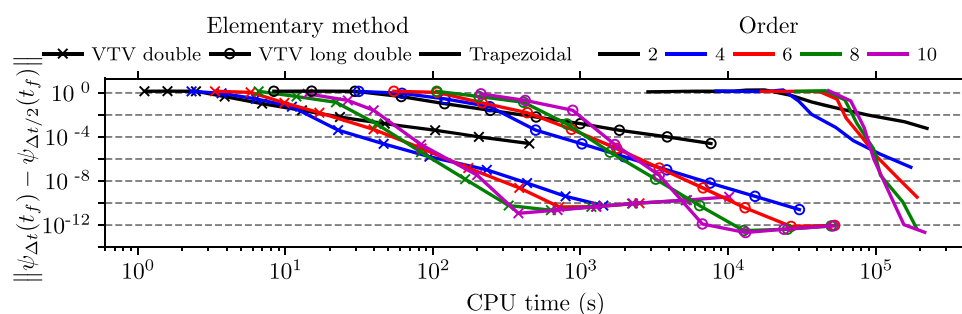


FIG. 11. Efficiency of the optimal compositions of the trapezoidal rule and VTV split-operator algorithm applied to the three-dimensional pyrazine model. For the trapezoidal rule, only the double precision version of the FFTW3 fast Fourier transform was used, while for the VTV split-operator algorithm, both double and long-double precision versions are compared. As for the fourth-order algorithms, Suzuki's fractal is considered as the "optimal" composition scheme.

mode. Therefore, the total number of grid points was increased to 32 768. The initial three-dimensional Gaussian wavepacket was obtained as the vibrational ground state of the ground-state potential energy surface ($q_0 = 0$, $p_0 = 0$ and $\sigma_0 = 1$ a.u. for each mode). Using the sudden approximation, employed also for the NaI model (see Sec. III of Paper I¹⁵), this initial wavepacket was then promoted to the second excited electronic state and the nonadiabatic quantum dynamics performed until a final time $t_f = 10\,000$ a.u. The population dynamics, shown in Fig. 10, indicates significant nonadiabatic transitions between the two excited states, while the ground surface remains unpopulated. Moreover, on the scale visible in the figure, the population dynamics obtained with sixth-order optimal compositions of the VTV algorithm and of the trapezoidal rule agree with each other.

Figure 11 compares the efficiency of different (yet always optimal) compositions of the VTV algorithm and trapezoidal rule. Higher-order integrators become more efficient already for convergence errors below 10^{-2} for compositions of the VTV algorithms and, remarkably, already for errors below 10^{-1} for compositions of the trapezoidal rule. In particular, to reach an error of 10^{-10} , a 900-fold speedup over the second-order VTV algorithm and a 300-fold speedup over the second-order trapezoidal rule are achieved by using their tenth-order optimal compositions. These results suggest that increasing the number of dimensions is either beneficial or, at the very least, not detrimental to the gain in efficiency from using the higher-order integrators. As in Fig. 7, the compositions of the VTV algorithms are much more efficient than the compositions of the trapezoidal rule, but this was expected because the Hamiltonian (15) is separable. One must remember that the main purpose of the compositions of the trapezoidal rule is for nonseparable Hamiltonians, where the split-operator algorithms cannot be used at all.

IV. CONCLUSION

We have described geometric integrators for nonadiabatic quantum dynamics in the diabatic representation, in which the Hamiltonian is separable into a kinetic term, depending only on momentum, and a potential term, depending only on position. These integrators are based on recursive symmetric composition of the standard, second-order split operator algorithm, and as a result, are explicit, unconditionally stable and exactly unitary, symplectic,

symmetric, and time-reversible. Unlike the original split-operator algorithm, which is only second-order, its recursive symmetric compositions can achieve accuracy of an arbitrary even order in the time step. These properties were justified analytically and demonstrated numerically on a diabatic two-surface model of NaI photodissociation. Indeed, the higher-order integrators sped up calculations by several orders of magnitude when higher accuracy was required. For example, the computational time required to achieve a convergence error of 10^{-10} was reduced by a factor of 600 when the optimal sixth-order composition was used instead of the elementary second-order split-operator algorithm. The gain in efficiency due to the higher-order integrators was also confirmed by the nonadiabatic simulations in a diabatic three-dimensional three-surface model of pyrazine. Although other efficient propagation methods, such as Chebyshev⁶⁹ or short iterative Lanczos schemes,^{38,39} might have comparable efficiency in this and other typical chemical systems, in contrast to the integrators presented here, those methods do not preserve time reversibility and several other geometric properties of the exact solution.

ACKNOWLEDGMENTS

The authors acknowledge the financial support from the European Research Council (ERC) under the European Union's Horizon 2020 research and innovation programme (Grant Agreement No. 683069—MOLEQULE) and from the Swiss National Science Foundation within the National Center of Competence in Research "Molecular Ultrafast Science and Technology" (MUST).

APPENDIX A: GEOMETRIC PROPERTIES OF NUMERICAL INTEGRATORS

To simplify many expressions, we set $\hbar = 1$ and denote the increment Δt with ϵ throughout this appendix. \hbar can be reintroduced by replacing each occurrence of t with t/\hbar (and ϵ with ϵ/\hbar). To analyze geometric properties of various integrators, we will use several well-known identities satisfied by the Hermitian adjoint and inverse operators, listed in Eqs. (A1)–(A4) of Paper I.¹⁵

1. Local error

The local error of an approximate evolution operator, defined as $\hat{U}_{\text{appr}}(\epsilon) - \hat{U}(\epsilon)$, is typically analyzed by comparing the

Taylor expansion of $\hat{U}_{\text{appr}}(\epsilon)$ with the Taylor expansion of the exact evolution operator

$$\hat{U}(\epsilon) = 1 - i\epsilon(\hat{T} + \hat{V}) - \frac{1}{2}\epsilon^2(\hat{T} + \hat{V})^2 + \mathcal{O}(\epsilon^3). \quad (\text{A1})$$

If the local error is $\mathcal{O}(\epsilon^{n+1})$, the method is said to be of order n because the global error for a finite time $t = P\epsilon$ is $\mathcal{O}(\epsilon^n)$.

The Taylor expansion of the TV algorithm (5) is

$$\begin{aligned} \hat{U}_{\text{TV}}(\epsilon) &= \left(1 - i\epsilon\hat{T} - \frac{1}{2!}\epsilon^2\hat{T}^2\right)\left(1 - i\epsilon\hat{V} - \frac{1}{2!}\epsilon^2\hat{V}^2\right) + \mathcal{O}(\epsilon^3) \\ &= 1 - i\epsilon(\hat{T} + \hat{V}) - \frac{1}{2}\epsilon^2(\hat{T}^2 + 2\hat{T}\hat{V} + \hat{V}^2) + \mathcal{O}(\epsilon^3) \\ &= \hat{U}(\epsilon) + \frac{1}{2}\epsilon^2[\hat{V}, \hat{T}] + \mathcal{O}(\epsilon^3), \end{aligned} \quad (\text{A2})$$

so the leading order local error is $\epsilon^2[\hat{V}, \hat{T}]/2$. Likewise, for the VT algorithm (4),

$$\hat{U}_{\text{VT}}(\epsilon) = \hat{U}(\epsilon) - \frac{1}{2}\epsilon^2[\hat{V}, \hat{T}] + \mathcal{O}(\epsilon^3). \quad (\text{A3})$$

The Taylor expansions of the second-order TVT and VTV algorithms are obtained by composing Taylor expansions (A2) and (A3) for time steps $\epsilon/2$, e.g.,

$$\begin{aligned} \hat{U}_{\text{TVT}}(\epsilon) &= \hat{U}\left(\frac{\epsilon}{2}\right)\hat{U}\left(\frac{\epsilon}{2}\right) + \frac{1}{8}\epsilon^2([\hat{V}, \hat{T}] - [\hat{V}, \hat{T}]) + \mathcal{O}(\epsilon^3) \\ &= \hat{U}(\epsilon) + \mathcal{O}(\epsilon^3). \end{aligned} \quad (\text{A4})$$

Equation (A4) and the same equation for $\hat{U}_{\text{VTV}}(\epsilon)$ demonstrate that both TVT and VTV are second-order algorithms.

2. Unitarity, symplecticity, and stability

Both first-order split-operator algorithms are unitary because

$$\begin{aligned} \hat{U}_{\text{TV}}(\epsilon)^{-1} &= e^{i\epsilon\hat{V}}e^{i\epsilon\hat{T}} = \hat{U}_{\text{TV}}(\epsilon)^\dagger, \\ \hat{U}_{\text{VT}}(\epsilon)^{-1} &= e^{i\epsilon\hat{T}}e^{i\epsilon\hat{V}} = \hat{U}_{\text{VT}}(\epsilon)^\dagger. \end{aligned}$$

Both second-order split-operator algorithms are unitary because they are compositions of unitary first-order algorithms.

Because the symplectic form was defined in Sec. II A as the imaginary part of the inner product and because VT, TV, VTV, and TVT algorithms as well as their compositions are unitary, all of them are also symplectic.

Stability follows from unitarity because

$$\|\psi(t + \epsilon) - \phi(t + \epsilon)\| = \|\psi(t) - \phi(t)\| \quad (\text{A5})$$

for unitary evolution operator $\hat{U}_{\text{appr}}(\epsilon)$. Since all split-operator methods are unitary, all are stable as well.

3. Commutation of the evolution operator with the Hamiltonian and conservation of energy

Because the kinetic and potential energy operators do not commute, unless $\hat{V} = \text{const}$, the evolution operator of no split-operator algorithm commutes with the Hamiltonian. For example, for the TV algorithm,

$$\begin{aligned} [\hat{H}, \hat{U}_{\text{TV}}(\epsilon)] &= [\hat{T} + \hat{V}, e^{-i\epsilon\hat{T}}e^{-i\epsilon\hat{V}}] \\ &= e^{-i\epsilon\hat{T}}[\hat{T}, e^{-i\epsilon\hat{V}}] + [\hat{V}, e^{-i\epsilon\hat{T}}]e^{-i\epsilon\hat{V}} \neq 0. \end{aligned} \quad (\text{A6})$$

As a consequence, split-operator algorithms do not conserve energy.

4. Symmetry and time reversibility

As shown, e.g., in Refs. 36 and 37 or in Appendix A of Paper I,¹⁵ the adjoint of an evolution operator satisfies the following properties:

$$(\hat{U}(\epsilon)^*)^* = \hat{U}(\epsilon), \quad (\text{A7})$$

$$(\hat{U}_1(\epsilon)\hat{U}_2(\epsilon))^* = \hat{U}_2(\epsilon)^*\hat{U}_1(\epsilon)^*, \quad (\text{A8})$$

$$\hat{U}(\epsilon)\hat{U}(\epsilon)^* \text{ is symmetric.} \quad (\text{A9})$$

Note that the third property gives a simple recipe for developing symmetric methods—by composing an arbitrary method and its adjoint, with both composition coefficients of 1/2.

The first-order VT and TV split-operator algorithms are adjoints of each other because

$$\hat{U}_{\text{TV}}(-\epsilon)^{-1} = e^{-i\epsilon\hat{V}}e^{-i\epsilon\hat{T}} = \hat{U}_{\text{VT}}(\epsilon) \quad (\text{A10})$$

and because of Eq. (A7). Therefore, neither VT or TV algorithm is symmetric or time-reversible. By contrast, the second-order VTV and TVT algorithms are both symmetric, which follows from Eq. (A9) applied to the two possible compositions of the VT and TV algorithms with composition coefficients 1/2. As shown, e.g., in Refs. 36 and 37 or in Appendix A of Paper I,¹⁵ time reversibility follows from symmetry. Therefore, both VTV and TVT algorithms and their symmetric compositions are time-reversible.

APPENDIX B: EXPONENTIAL CONVERGENCE WITH GRID DENSITY

The top panel of Fig. 12 exhibits the exponential convergence of the molecular wavefunction with the increasing number of grid points for the NaI model in the diabatic basis. The ranges as well

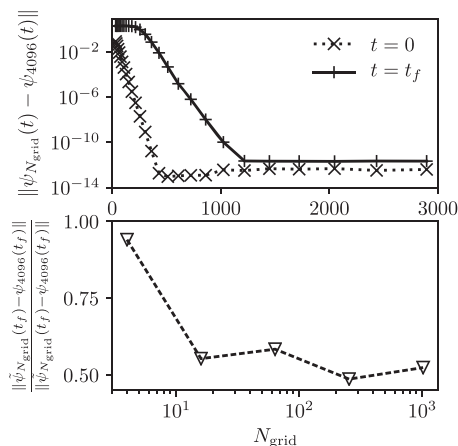


FIG. 12. Top: Convergence of the initial and final wavepackets with the increasing number of grid points. Bottom: Ratio of the integration error and total convergence error at the final time as a function of the number of grid points. (See Appendix B for details.) The sixth-order optimal composition of the VTV algorithm with time step $\Delta t = t_f/2^7$ was used for propagation.

as the densities of both the position and momentum grids were increased by a factor of $\sqrt{2}$ for each increase in the number N_{grid} of grid points by a factor of two. Convergence error required comparing wavefunctions on grids with different densities, which was carried out by trigonometric interpolation of the wavefunction on the sparser grid. Increasing N_{grid} reduces the convergence error at time t_f (top panel) because the errors of both the required overlap integral and of the propagation decrease. To compare these two effects, the bottom panel of Fig. 12 shows the ratio of the purely integration error and the total error. The integration error is defined as $\|\tilde{\Psi}_{N_{\text{grid}}}(t_f) - \Psi_{4096}(t_f)\|$, where $\Psi_{4096}(t_f)$ is the wavefunction propagated on the fully converged grid and $\tilde{\Psi}_{N_{\text{grid}}}(t_f)$ is $\Psi_{4096}(t_f)$ represented with N_{grid} grid points. In other words, the representation on a reduced grid is done only after propagation. The panel shows that at the final time, the integration error is approximately one half of the total error. Therefore, the integration and propagation errors due to a finite grid are similar.

REFERENCES

- M. Born and R. Oppenheimer, *Ann. Phys.* **389**, 457 (1927).
- E. J. Heller, *The Semiclassical Way to Dynamics and Spectroscopy* (Princeton University Press, Princeton, NJ, 2018).
- A. Mokhtari, P. Cong, J. L. Herek, and A. H. Zewail, *Nature* **348**, 225 (1990).
- M. Baer, *Beyond Born-Oppenheimer: Electronic Nonadiabatic Coupling Terms and Conical Intersections*, 1st ed. (Wiley, 2006).
- H. Nakamura, *Nonadiabatic Transition: Concepts, Basic Theories and Applications*, 2nd ed. (World Scientific Publishing Company, 2012).
- K. Takatsuka, T. Yonehara, K. Hanasaki, and Y. Arasaki, *Chemical Theory beyond the Born-Oppenheimer Paradigm: Nonadiabatic Electronic and Nuclear Dynamics in Chemical Reactions* (World Scientific, Singapore, 2015).
- M. P. Bircher, E. Liberatore, N. J. Browning, S. Brickel, C. Hofmann, A. Patoz, O. T. Unke, T. Zimmermann, M. Chergui, P. Hamm, U. Keller, M. Meuwly, H. J. Woerner, J. Vaniček, and U. Rothlisberger, *Struct. Dyn.* **4**, 061510 (2017).
- S. Shin and H. Metiu, *J. Chem. Phys.* **102**, 9285 (1995).
- Al. Albert, D. Kaiser, and V. Engel, *J. Chem. Phys.* **144**, 171103 (2016).
- E. Mátyus, *Mol. Phys.* **117**, 590 (2019).
- A. Abedi, N. T. Maitra, and E. K. Gross, *Phys. Rev. Lett.* **105**, 123002 (2010).
- L. S. Cederbaum, *J. Chem. Phys.* **128**, 124101 (2008).
- T. Zimmermann and J. Vaniček, *J. Chem. Phys.* **132**, 241101 (2010).
- T. Zimmermann and J. Vaniček, *J. Chem. Phys.* **136**, 094106 (2012).
- S. Choi and J. Vaniček, *J. Chem. Phys.* **150**, 204112 (2019).
- M. Ben-Nun, J. Quenneville, and T. J. Martínez, *J. Phys. Chem. A* **104**, 5161 (2000).
- B. F. E. Curchod and T. J. Martínez, *Chem. Rev.* **118**, 3305 (2018).
- D. V. Shalashilin and M. S. Child, *J. Chem. Phys.* **115**, 5367 (2001).
- D. V. Makhov, C. Symonds, S. Fernandez-Alberti, and D. V. Shalashilin, *Chem. Phys.* **493**, 200 (2017).
- G. A. Worth, M. A. Robb, and I. Burghardt, *Faraday Discuss.* **127**, 307 (2004).
- G. Richings, I. Polyak, K. Spinlove, G. Worth, I. Burghardt, and B. Lasorne, *Int. Rev. Phys. Chem.* **34**, 269 (2015).
- H.-D. Meyer, U. Manthe, and L. S. Cederbaum, *Chem. Phys. Lett.* **165**, 73 (1990).
- G. A. Worth, H.-D. Meyer, H. Köppel, L. S. Cederbaum, and I. Burghardt, *Int. Rev. Phys. Chem.* **27**, 569 (2008).
- H. Wang and M. Thoss, *J. Chem. Phys.* **119**, 1289 (2003).
- G. Avila and T. Carrington, Jr., *J. Chem. Phys.* **147**, 144102 (2017).
- C. Lubich, *From Quantum to Classical Molecular Dynamics: Reduced Models and Numerical Analysis*, 12th ed. (European Mathematical Society, 2008).
- G. A. Worth and L. S. Cederbaum, *Annu. Rev. Phys. Chem.* **55**, 127 (2004).
- W. Domcke and D. R. Yarkony, *Annu. Rev. Phys. Chem.* **63**, 325 (2012).
- C. A. Mead and D. G. Truhlar, *J. Chem. Phys.* **77**, 6090 (1982).
- G. Granucci, M. Persico, and A. Toniolo, *J. Chem. Phys.* **114**, 10608 (2001).
- H. Nakamura and D. G. Truhlar, *J. Chem. Phys.* **117**, 5576 (2002).
- M. Baer, *Phys. Rep.* **358**, 75 (2002).
- H. Koppel, W. Domcke, and L. S. Cederbaum, *Adv. Chem. Phys.* **57**, 59 (1984).
- M. D. Feit, J. A. Fleck, Jr., and A. Steiger, *J. Comput. Phys.* **47**, 412 (1982).
- D. J. Tannor, *Introduction to Quantum Mechanics: A Time-Dependent Perspective* (University Science Books, Sausalito, 2007).
- E. Hairer, C. Lubich, and G. Wanner, *Geometric Numerical Integration: Structure-Preserving Algorithms for Ordinary Differential Equations* (Springer Berlin Heidelberg, New York, 2006).
- B. Leimkuhler and S. Reich, *Simulating Hamiltonian Dynamics* (Cambridge University Press, 2004).
- C. Lanczos, *J. Res. Nat. Bur. Stand.* **45**, 255 (1950).
- T. J. Park and J. C. Light, *J. Chem. Phys.* **85**, 5870 (1986).
- A. I. Kuleff, J. Breidbach, and L. S. Cederbaum, *J. Chem. Phys.* **123**, 044111 (2005).
- E. Forest and R. D. Ruth, *Physica D* **43**, 105 (1990).
- M. Suzuki, *Phys. Lett. A* **146**, 319 (1990).
- H. Yoshida, *Phys. Lett. A* **150**, 262 (1990).
- A. D. Bandrauk and H. Shen, *Chem. Phys. Lett.* **176**, 428 (1991).
- A. D. Bandrauk, E. Dehghanian, and H. Lu, *Chem. Phys. Lett.* **419**, 346 (2006).
- T. Prosen and I. Pižorn, *J. Phys. A* **39**, 5957 (2006).
- H. De Raedt, *Comput. Phys. Rep.* **7**, 1 (1987).
- M. Suzuki, *Phys. Lett. A* **201**, 425 (1995).
- S. A. Chin and C. R. Chen, *J. Chem. Phys.* **117**, 1409 (2002).
- R. I. McLachlan, *SIAM J. Sci. Comput.* **16**, 151 (1995).
- M. Wehrle, M. Šulc, and J. Vaniček, *Chimia* **65**, 334 (2011).
- J. Crank and P. Nicolson, *Math. Proc. Cambridge Philos. Soc.* **43**, 50 (1947).
- E. A. McCullough, Jr. and R. E. Wyatt, *J. Chem. Phys.* **54**, 3578 (1971).
- V. Engel and H. Metiu, *J. Chem. Phys.* **90**, 6116 (1989).
- G. Stock, C. Woywod, W. Domcke, T. Swinney, and B. S. Hudson, *J. Chem. Phys.* **103**, 6851 (1995).
- P. R. Halmos, *Finite Dimensional Vector Spaces* (Princeton University Press, 1942).
- M. Creutz and A. Gocksch, *Phys. Rev. Lett.* **63**, 9 (1989).
- W. Kahan and R.-C. Li, *Math. Comput.* **66**, 1089 (1997).
- M. Sofroniou and G. Spalletta, *Optim. Methods Software* **20**, 597 (2005).
- H. F. Trotter, *Proc. Am. Math. Soc.* **10**, 545 (1959).
- G. Strang, *SIAM J. Numer. Anal.* **5**, 506 (1968).
- R. Kosloff and D. Kosloff, *J. Chem. Phys.* **79**, 1823 (1983).
- D. Kosloff and R. Kosloff, *J. Comput. Phys.* **52**, 35 (1983).
- M. Frigo and S. G. Johnson, *Proc. IEEE* **93**, 216 (2005).
- G. H. Golub and C. F. Van Loan, *Matrix Computations*, 3rd ed. (The Johns Hopkins University Press, 1996).
- R. B. Sidje, *ACM Trans. Math. Software* **24**, 130 (1998).
- E. Anderson, Z. Bai, C. Bischof, S. Blackford, J. Demmel, J. Dongarra, J. Du Croz, A. Greenbaum, S. Hammarling, A. McKenney, and D. Sorensen, *LAPACK Users' Guide*, 3rd ed. (Society for Industrial and Applied Mathematics, 1999).
- C. Woywod, W. Domcke, A. L. Sobolewski, and H. Werner, *J. Chem. Phys.* **100**, 1400 (1994).
- H. Tal-Ezer and R. Kosloff, *J. Chem. Phys.* **81**, 3967 (1984).